Edge dislocations in fcc metals: Microscopic calculations of core structure and positron states in Al and Cu

H. Häkkinen, S. Mäkinen, and M. Manninen

Department of Physics, University of Jyväskylä, SF-40100 Jyväskylä 10, Finland

(Received 27 November 1989; revised manuscript received 23 March 1990)

Structures of edge dislocations (dislocation line direction $[1\bar{1}2]$, Burgers vector $(a/2)[110]$) in aluminum and copper are studied with the molecular-dynamics simulation method which incorporates the effective-medium theory extended to include atomic interactions beyond the nearest neighbors. The observed equilibrium distance between the Shockley partial dislocations in both metals agrees well with the estimate evaluated from elasticity theory by using known values for the stacking-fault energy and the bulk modulus. Effective-medium theory leads to a dislocation core which is narrower than the previous results of the pair-potential calculations for simple metals. The vacancy formation energy in copper is higher at the center of the stacking-fault region than in the bulk, which suggests that pipe diffusion can take place only in the narrow partial dislocation core. In the second part of the work, the role of the dislocation line and of the associated point defects as positron traps are studied in both metals. The pure dislocation line forms only a shallow trap but it can be a precursor state for deeper traps, like vacancies and single jogs on the dislocation line. The calculated lifetimes for these defects are in good agreement with the experimentally observed lifetime components coming from dislocations.

I. INTRODUCTION

Dislocations have their well-known effects on the plastic behavior and crystal growth of materials.[1] Moreover, their role as fast diffusion channels[2] and in the theory of melting transition[3] have been a subject of active debate. The first theoretical models for dislocations were based on the elastic continuum theory, which can well describe the long-range stress fields formed in the lattice by the presence of dislocations.[4] However, the elasticity theory breaks up in the dislocation core, where the inelastic atom-atom interactions become dominant. Because of the lack of experimental tools in the atomic scale, the available information about the atomic arrangements in the core region has been mainly resulted from computer simulations.[5] The atomic interactions have usually been described in these simulations by pair potentials, which have been either empirical or derived from the pseudopotential theory.[6] However, pair potentials have many serious shortcomings in description of the metallic cohesion and of defect structures in metals. This is true also in the case of dislocation cores containing pointlike defects, such as vacancies, jogs and kinks. In real samples dislocations act as sinks for these defects.

During the 1980s there has been a significant development in the derivation of interatomic potentials suitable for computer simulations of metals. The main idea has been to extend the "effective-medium" or "quasiatom" scheme of cohesion, originally used in the description of an impurity in a metallic environment,[7] and apply it to the whole lattice by considering each metal atom as an "impurity" with the respect to all other metal atoms. This extension leads to the total cohesive energy[8]

$$E_{\text{tot}} = \sum_{i=1}^{N} F_i(n_i) + \frac{1}{2} \sum_{\substack{i,j=1 \\ (j \neq i)}}^{N} V(r_{ij}) , \qquad (1)$$

where F_i is the embedding energy of atom i, n_i is the local electron density at the atomic site i (provided by the neighboring atoms), V is a pair potential, and N is the number of metal atoms. n_i depends on the distances r_{ij} between neighboring atoms, and in this way F_i is structure dependent and implicitly includes many-atom interactions. Various models[9-12] now use this scheme of cohesion, each of which gives a slightly different derivation of and interpretation to the components in Eq. (1). The many-atom interactions can explain many properties inherent in metals, like the usual inward relaxation of the surface layer, the low vacancy formation energy with respect to the cohesive energy, and the relations between the elastic constants. Many-atom models can then be expected to give a more reliable picture also of the structure of dislocations and grain boundaries.[6,13-15]

The atomic positions around the dislocation core can be studied experimentally by, e.g., transmission- or high-resolution electron microscopes[16,17] and positron-annihilation techniques.[18,19] First evidences of positron trapping in deformed metals appeared about twenty years ago,[20,21] and since then several experiments have been done with samples containing dislocations.[22-24] Different kinds of theories have been suggested to explain the results of these experiments. In the early 1970s Martin and Paetsch used elasticity theory to calculate the atomic positions on the dislocation line, and pair potential to describe the interaction between the positron and the Al ions.[25] They concluded that the dislocation line in

Al is only a very shallow trap for positrons with a binding energy of less than 100 meV. Also Doyama and Cotterill[26] and Smedskjaer et al.[27] suggested that the pure dislocation line is a weak positron trap, and explained the long lifetimes seen in experiments by pointlike defects (vacancies, jogs) associated with the dislocation. On the other hand, Bergensen and McMullen,[28] and Arponen et al.[29] assumed that the pure dislocation line is a strong positron trap and could find reasonable agreement with the experimental data, too.

In this paper we give the results of a microscopic calculation of edge dislocation structures in aluminum and copper. We have studied the structure of an extended $(a/2)[1\bar{1}0]$ edge dislocation (both the pure dislocation line and the point defects associated with it) using the molecular-dynamics and the effective-medium theory (EMT).[9] The EMT includes many-atom interactions and is based on ab initio calculations of the atom in a homogeneous electron gas. We start by studying the equilibrium separation of the two partial dislocations and the core structure of the extended dislocation. The equilibrium separation we find is in agreement with the estimate from the elasticity theory. The present many-atom interactions result in a core region which is narrower than those found in the earlier pair-potential simulations. In the second part of the paper we shall study the interaction of positrons with the defect structures obtained form molecular-dynamics simulations. The method used in the positron-state calculations have previously been proved to give a reliable description of the positron-annihilation characteristics in a wide variety of crystal defects, both in metals and in semiconductors.[30,31] The comparison of the calculated lifetimes with the experimentally measured lifetimes in plastically deformed metal samples clearly indicates that the pure dislocation line is only a shallow trap, whereas the observed long lifetimes come from positrons trapped at vacancies or jogs in the dislocation core.

In Sec. II we shall briefly describe the atomic interaction model which is used in the molecular-dynamics simulations. The model and method of calculating the positron states are described in Sec. III. The results of the molecular-dynamics simulations for the core structure of the extended dislocation are discussed in Sec. IV, and the results for the positron annihilation in dislocations in Sec. V. Section VI contains our conclusions.

II. THE EFFECTIVE-MEDIUM THEORY

The nearest-neighbor formalism of the EMT has been described in detail by Jacobsen et al.[9] It has been proved to be successful in describing many properties of fcc metals, such as the structure of a pure metal surface or an adsorbate-surface system, and the high-temperature dynamics of a metal surface.[9,32] However, it cannot be applied directly to extended dislocations, because it does not have any energy of formation for the stacking fault between the two partial dislocations. We have followed the outlines of Jacobsen et al.[9] to extend the range of the atomic interactions beyond the nearest neighbors. We have tested the extended theory by simulating the thermal behavior of bulk copper. We found that the ex-

tended model describes well the thermal expansion and melting.[33] This section shortly reviews the physical picture in EMT. The parametrization of the potential, which has been used in the molecular-dynamic simulations, is given in Ref. 33.

The approach of Jacobsen et al.[9] is based on the ansatz that the total electron density of a metallic system (composed of N atoms) can be written as a superposition of free-atom-likes densities $\Delta n_i(\mathbf{r})$,

$$n(\mathbf{r}) = \sum_{i=1}^{N} \Delta n_i(\mathbf{r}) , \tag{2}$$

where $\Delta n_i(\mathbf{r})$ is an electron density induced in a homogeneous electron gas by the presence of atom i. In the calculation of the electron densities EMT makes the so-called atomic-sphere approximation, where the system is composed of atomic spheres centered at the fcc-lattice sites. The radius of a sphere is determined by the requirement that the sphere is electrically neutral. In the lattice in equilibrium this definition is the same as that of a spherical Wigner-Seitz cell associated with each atom. The requirement of neutrality produces a unique relationship between the radius of a given atomic sphere s_i and the embedding electron density at the corresponding lattice site $\bar{n}_i$. The embedding density at each lattice site can be calculated from the positions of neighboring atoms. For each element there is an optimum embedding density n_0, which determines the equilibrium lattice constant of its solid phase.

The total binding energy of a metallic system is now written as

$$E_{\text{tot}} = \sum_{i=1}^{N} E_{C,i}(\bar{n}_i) + \Delta E_{1\text{el}} + \Delta E_{\text{AS}} . \tag{3}$$

In this expression the main contribution to the cohesion energy comes from the first term on the right-hand side. The second and the third term are corrections, which will be defined at the end of Sec. II. The density-dependent energy function $E_{C,i}$ is defined as

$$E_{C,i}(\bar{n}_i) = E_i^{\text{hom}}(\bar{n}_i) - \alpha(\bar{n}_i)\bar{n}_i , \tag{4}$$

where $E_i^{\text{hom}}(\bar{n}_i)$ is the embedding energy of atom i in a homogeneous electron gas of density $\bar{n}_i$, and $\alpha(\bar{n}_i)$ is an integral of the induced electrostatic potential $\Delta\phi$ over a neutral sphere of radius s_i,

$$\alpha(\bar{n}_i) = \int_{s_i} \Delta\phi(\mathbf{r})d\mathbf{r} . \tag{5}$$

The subscript i is written explicitly to indicate that the local electron density depends on the atomic site. The cohesive function $E_C(\bar{n})$ has been calculated by Puska et al.[34] for a large number of elements. These functions are unique in the sense that the same function can be used for a given element both in a pure metal or in an alloy. Qualitatively, the form of the cohesive function is related to the chemical activity of the element: the inert gases have a linear repulsive E_C, but in other elements E_C usually has a single minimum. This minimum is a result of competition between the kinetic repulsion, which dominates in the embedding function E^{hom}, and the electrostatic attraction $-\alpha(\bar{n})\bar{n}$. In the density region usually found in

metals, E_C functions are parametrized with third-order polynomials,[9] where the zeroth-order coefficient is (by definition) the equilibrium cohesive energy per atom, and the second-order coefficient is related to the bulk modulus.

The second term in Eq. (3) is the correction to the cohesion energy coming from one-electron energy levels. This correction is important in transition metals, which have partially filled d bands (and many of them have a bcc structure). For nontransition metals like aluminum and noble metals this one-electron energy correction is assumed to be small.

The third term in Eq. (3) is the so-called atomic-sphere correction. It arises from the fact that the neighboring Wigner-Seitz spheres begin to overlap when atoms are distorted away from their equilibrium positions. This overlap energy is defined to be

$$E_{AS} = -\frac{1}{2} \int O(\mathbf{r}) n(\mathbf{r}) \phi(\mathbf{r}) d\mathbf{r} , \qquad (6)$$

where $n(\mathbf{r})$ and $\phi(\mathbf{r})$ are the total electron density and the electrostatic potential potential, respectively, and $O(\mathbf{r})$ is the overlap function, $O(\mathbf{r}) = m - 1$, where m is the number of overlapping spheres at point $\mathbf{r}$. The atomic-sphere correction for atom i consists approximately of the electrostatic interaction $a\bar{n}_i$ and of a sum of pair interactions $V(r_{ij})$, as shown in Ref. 9.

If the one-electron energy correction is neglected (which can be done, e.g., in the case of simple metals and noble metals), the binding energy expression in EMT (3) can be written as a sum of a density-dependent many-atom term and a pair term [Eq. (1)]. The basic difference between EMT and other novel many-atom schemes[10–12] is that nearly all parameters needed in EMT can be *calculated* in the framework of the density-functional theory. The parametrization of the "embedded-atom method" (EAM),[10] the "Finnis-Sinclair (FS) model,"[11] and the "glue model"[12] is based on empirical fitting, although the functional forms used in EAM and FS models also have theoretical background. The relationship between EAM, FS, and EMT models has been studied in more detail by Johnson.[35]

III. CALCULATION OF POSITRON STATES

The potential seen by the positron, its wave function, and annihilation characteristics in a given atomic arrangement have been calculated using the method of Puska and Nieminen.[30] This method is based on non-self-consistent electron structures, which makes it much less time consuming than the simultaneous self-consistent calculation of the electron density and the positron state. Model calculations, which have been made by the two-component density-functional theory (DFT) (Refs. 36 and 37) for the positron localized in a metal vacancy,[38] show that the self-consistency of the electron structure changes

the positron annihilation rate only slightly. For a nonlocalized positron in a perfect metal host the difference in positron lifetimes is even smaller because the non-self-consistent superposition of free atoms used in the present method reproduces rather well the electron density and the open volume in the interstitial regions. In the case of a perfect host these are indeed the most important aspects of the positron-state calculations, because, due to the strong repulsion from the ion cores, the positron wave function is mainly localized in the interstitial regions between the ions.

Positron-state calculations are started by solving the electrostatic potential and the electron density of a free host atom. In calculating the electronic structure we use the DFT with the Ceperley-Alder[39] exchange-correlation function as parametrized by Perdew and Zunger. The fully three-dimensional Coulomb potential V_{Coulomb} and the electron density n^- seen by the positron in the host are then obtained by placing these free atoms to the points $\mathbf{R}_i$ determined by the molecular-dynamics simulation:

$$V_{\text{Coulomb}}(\mathbf{r}) = \sum_i V_{\text{at}}(|\mathbf{r} - \mathbf{R}_i|) ,$$

$$n^-(\mathbf{r}) = \sum_i n_{\text{at}}^-(|\mathbf{r} - \mathbf{R}_i|) . \qquad (7)$$

Here $V_{\text{at}}(r)$ and $n_{\text{at}}^-(r)$ are the spherically symmetric electrostatic potential and the electron density of a free atom at distance r, respectively.

The positron potential V_+ entering the corresponding Schrödinger equation consists of an electrostatic part, V_{Coulomb} of Eq. (7), and a correlation potential V_{corr}, which is caused by the interactions between the positron and the host electrons. The correlation potential is estimated from the many-body calculations of Arponen and Pajanne[40] for a positron in homogeneous electron gas. The local-density approximation is used in determining V_{corr}, and the total potential is

$$V_+(\mathbf{r}) = V_{\text{Coulomb}}(\mathbf{r}) + V_{\text{corr}}(n^-(\mathbf{r})) . \qquad (8)$$

Here n^- is the undisturbed electron density, which means that V_{corr} corresponds to the low positron density limit of the effective positron potential which is used in the two-component DFT. The present method is thus correct in the low positron density limit of the two-component formalism.

The potential of Eq. (8) is calculated at the nodes of a three-dimensional mesh which forms an orthorhombic Bravais lattice. The Schrödinger equation is discretized, and the positron wave function and its energy eigenvalue are solved iteratively at the mesh points by a numerical relaxation method.[41,42] In the nth iteration loop the energy eigenvalue $\varepsilon^{(n)}$ is obtained from the corresponding positron wave function and the potential as

$$\varepsilon^{(n)} = \sum_{i,j,k} \left[\psi_{ijk}^{(n)} \left[-\frac{1}{2h_1^2} (\psi_{i+1,j,k}^{(n)} - 2\psi_{ijk}^{(n)} + \psi_{i-1,j,k}^{(n)}) - \frac{1}{2h_2^2} (\psi_{i,j+1,k}^{(n)} - 2\psi_{ijk}^{(n)} + \psi_{i,j-1,k}^{(n)}) \right. \right.$$

$$\left. \left. - \frac{1}{2h_3^2} (\psi_{i,j,k+1}^{(n)} - 2\psi_{ijk}^{(n)} + \psi_{i,j,k-1}^{(n)}) \right] + V_{ijk} |\psi_{ijk}^{(n)}|^2 \right] \Big/ \sum_{i,j,k} |\psi_{ijk}^{(n)}|^2 , \qquad (9)$$

in atomic units. Here $\psi_{ijk}^{(n)}$ is the positron wave function at mesh point (i,j,k), h_l $(l=1,2,3)$ is the separation between two adjacent mesh points in the lth direction (perpendicular to each other), and V_{ijk} is the positron potential at point (i,j,k). As the initial value of the positron wave function we use a cosinelike function which has its maximum value in the middle of the three-dimensional calculation mesh. In the $(n+1)$th iteration loop the wave function is calculated from the discretized Schrödinger equation as

$$\psi_{ijk}^{(n+1)} = \frac{\frac{1}{2h_1^2}(\psi_{i-1,j,k}^{(n)} + \psi_{i+1,j,k}^{(n)}) + \frac{1}{2h_2^2}(\psi_{i,j-1,k}^{(n)} + \psi_{i,j+1,k}^{(n)}) + \frac{1}{2h_3^2}(\psi_{i,j,k-1}^{(n)} + \psi_{i,j,k+1}^{(n)})}{\frac{1}{h_1^2} + \frac{1}{h_2^2} + \frac{1}{h_3^2} + V_{ijk} - \varepsilon^{(n)}}, \tag{10}$$

in atomic units. The calculation is finished when the energy eigenvalue does not change in two consecutive iteration loops.

The positron-annihilation rate, the inverse of the lifetime, is given by[30]

$$\lambda = \pi r_0^2 c \int d\mathbf{r} |\psi(\mathbf{r})|^2 [n_v(\mathbf{r})\gamma_v(n_v(\mathbf{r}))$$
$$+ n_d(\mathbf{r})\gamma_d + n_c(\mathbf{r})\gamma_c], \tag{11}$$

where r_0 is the classical radius of electron, c is the velocity of light, n_v, n_d, and n_c are the valence-electron, d-electron, and core-electron densities, respectively. $\gamma_v(n)$ is the Brandt-Reinheimer[43] enhancement factor for the valence electrons. γ_d and γ_c are the enhancement factors for the d electrons and core electrons, respectively. For these we have used the values given by Puska and Nieminen.[30]

IV. MOLECULAR-DYNAMICS RESULTS FOR THE EXTENDED EDGE DISLOCATION

Energetically, the most favored perfect (undissociated) edge dislocation in fcc metals has dislocation line direction $\langle 112 \rangle$ and Burgers vector $\mathbf{b}=(a/2)\langle 110 \rangle$ (in units of the lattice parameter). However, this kind of perfect dislocation does not occur in metals, because it can reduce its elastic energy by dissociating into two Shockley partial dislocations according to the scheme[44]

$$\mathbf{b} \rightarrow \mathbf{b}_1 + \mathbf{b}_2,$$
$$(a/2)\langle 110 \rangle \rightarrow (a/6)\langle 211 \rangle + (a/6)\langle 12\bar{1} \rangle. \tag{12}$$

The partial Burgers vectors $\mathbf{b}_1$ and $\mathbf{b}_2$ lie in the same (111) plane, which means that the partial dislocations are likely to glide in that plane, but they cannot climb. Here we define the glide plane to be that (111) plane which contains the partial dislocation lines. We use also the concept of slip plane. This is a virtual (not atomic) plane between the glide plane and the adjacent (111) plane with missing atoms. The dissociation of the perfect dislocation changes the stacking sequence of the (111) planes between the partials. The equilibrium separation of the partials is determined by the balance between the repulsive elastic force and the attractive force coming from the stacking fault. In this section we present molecular-dynamics results for the dissociation of the perfect dislocation to Shockley partial dislocations and for the relaxed structure of the partial dislocation pair, which is called the "extended dislocation." This spontaneous dissociation and the relaxed structure can be reliably simulated only if the atomic interaction model is capable of giving a reasonable energy for the formation of the stacking fault. The stacking-fault energies calculated from the extended EMT for aluminum and copper are discussed in Sec. IV A. The molecular-dynamics simulations of the dissociation of the perfect dislocation and the resulting extended dislocation are discussed in Sec. IV B. The earlier studies of the extended dislocations in fcc metals have not usually been fully dynamical calculations, but based on various relaxation methods and on a very careful adjustment of the boundary conditions during the dissociation. Here we show the power of the molecular dynamics to spontaneously create the dynamical equilibrium between the partials. We can exclude the effects of the boundary conditions on our results by using large sample sizes and two qualitatively different simulation geometries: the rod geometry and the bulk geometry. Simulations with the bulk geometry lead to an edge dislocation dipole and are discussed in Sec. IV C. The real dislocations are always accompanied with pointlike defects in the dislocation core: vacancies, interstitials, jogs, and kinks. We have studied the relaxation of a vacancy on the dislocation line and in the stacking-fault region. The results of these simulations are discussed in Sec. IV D with reference to the renewed interest in the pipe diffusion in dislocations.[45]

A. Calculation of the stacking-fault energy

The energy of the stacking fault is calculated with a cell of eight close-packed (111) layers of 36 atoms containing an intrinsic unrelaxed stacking fault with the sequence $ABCBCABC$. Periodic-boundary conditions are imposed in all directions, so the sample is a portion of a bulk crystal with an infinite stacking-fault plane.[46] The lattice parameter of the crystal is equal to its zero-temperature value which is an outcome of the EMT: 7.68 a.u. for Al and 6.60 a.u. for Cu. The stacking-fault energy γ is then determined by

$$\gamma = \frac{E' - NE_0}{A}, \tag{13}$$

where E' is the total potential energy of the sample containing the stacking fault, N is the number of atoms in the cell (288), E_0 is the cohesive energy per atom, and A is the area of the (111) plane. The results for Al and Cu calculated with various ranges of interactions are present-

TABLE I. The formation energy γ for an unrelaxed stacking fault in aluminum and copper calculated from the effective-medium theory. The cutoff radius is given with numbers $\frac{3}{4}, \frac{4}{5} \ldots$, to show whether the range of the interactions has been in the middle of third and fourth, fourth and fifth, etc. neighbors in the fcc lattice. The stacking-fault energies are in units of ergs/cm². The last line shows the range of the experimentally estimated values (Refs. 44 and 47) for γ.

Cutoff	γ(Al) (ergs/cm²)	γ(Cu) (ergs/cm²)
$\frac{3}{4}$	55	79
$\frac{4}{5}$	−9	−13
$\frac{5}{6}$	7	7
$\frac{6}{7}$	−14	−17
expt.	140–200	30–80

ed in Table I together with experimentally observed values.[44,47] In the present scheme of cohesion, the stacking-fault energy is determined by the atomic sphere correction [the last term in Eq. (3)], because the one-electron energy correction is neglected, and the cohesive function E_C is not sensitive to small structural changes.

The stacking-fault energy we find for Cu agrees very well with the experimental results, provided the interactions are extended to the third nearest neighbors in the fcc lattice. The oscillating behavior of stacking-fault energy as a function of the interaction range is, in fact, no surprise. A similar sensitivity to the range of the interactions has been found also for empirical pair potentials and pseudopotentials[47] In the case of EMT, one can argue that the exponential approximation of the density tails[9] is not a good description for the true induced densities far from the atom, where the Friedel oscillations may play a role. The calculated stacking-fault energy for Al is about one-third of the experimental value. It is worth noticing that the fcc metals with high stacking-fault energies, such as Al and Ni, appear to be problematic as well in the other novel many-atom models[15] as in many empirical pair potentials.[47] Some success has been achieved in calculating the stacking-fault energy of aluminum using pseudopotentials.[48] It can be expected that the main contribution to the stacking-fault energy comes from the redistribution of the valence-electron density and the related modification of the Fermi surface near the zone boundaries. In aluminum these modifications are much more significant than in a monovalent metal like copper, which has a nearly free-electron Fermi sphere. Nickel, on the other hand, has an incomplete d band, which may indicate the importance of directional effects in the stacking fault region. The simple spherical averaging made in the calculation of electron densities in EMT cannot account for the effects coming from the modified Fermi surface or from directional bonding.

In addition to the static calculations of the unrelaxed stacking fault, the effects of relaxations were determined for aluminum with a molecular dynamics run of 6 ps. The three layer-by-layer distances within the $BCBC$ se-

quence inside the fcc crystal were found to increase by 0.3%, 0.8%, and 0.3%, respectively. This result is in agreement with the results of Cotterill and Doyama,[47] who found similar increase of the lattice spacing in the stacking fault region.

In the rest of the paper the atomic interactions are extended only to the third neighbors in order to guarantee a reliable energy for the stacking fault.

B. Structure of the extended dislocation

The preparation of the sample which contains a perfect edge dislocation is started with an ideal fcc crystal defined in the real space by the lattice vectors $8a[\bar{1}11]$, $(3a/2)[1\bar{1}2]$, and $28a[110]$, which form the x, y, and z edges of the simulation cell, respectively. The numbers of primitive cells in the x, y, and z directions are then 8, 3, and 56. This means that the number of $(\bar{1}11)$, $(1\bar{1}2)$, and (110) planes are 24, 18, and 112, respectively, and the total number of atoms is 8064. The density of the sample is set equal to the zero-temperature lattice which is determined by the effective medium theory. After that, two adja- cent (110) half-planes are removed in the middle of the sample resulting in the stacking sequence $\ldots ABAB\square\square ABAB \ldots$ ($\square$ stands for the missing plane). One half-plane is further moved by one lattice spacing resulting in the structure $\ldots ABAB\square A\square BAB \ldots$. All atoms are then displaced according to the linear elasticity theory,[4] and the resulting configuration is the starting point for the molecular-dynamics simulations. Simulations are made with a modified rod geometry, the only periodic direction being the dislocation line direction $[1\bar{1}2]$. The two $(\bar{1}11)$ surfaces of the sample are free, but three atomic layers on the two (110) surfaces are fixed at the positions calculated from the linear elasticity theory, resulting in an asymptotically constant elastic stress imposed on the partials. The resulted configuration of 7992 atoms (from which 7560 dynamical) is the starting point for the constant-volume (microcanonical) molecular dynamics. The Newtonian equations for the atoms are solved by a third-order predictor-corrector algorithm[49] with a time step of 3 fs for both Al and Cu. The lengths of the runs have been 4000 time steps which corresponds to 12 ps in real time.

The dissociation of the perfect dislocation was found to take place immediately after the dynamical calculation was started. The kinetic energy of the atoms was removed after each 10 time steps (0.03 ps) to allow the system to relax to the equilibrium structure. Dissociation was completed in about 4 ps in both simulations, and the separation distance of the partial dislocations remained constant thereafter. We have determined the average system structure during the time interval of 2000–4000 time steps (6–12 ps), when the temperature has been of the order of 10^{-3} K, which means that the contribution of the kinetic energy to the total energy is vanishingly small, and the average positions of the atoms coincide with their zero-temperature positions.

We illustrate the structure of the extended dislocation in copper in Fig. 1(a), which shows the average atomic

positions in the $(\bar{1}11)$ planes above and below the slip plane. The different stacking in the middle of the partials is clearly seen. The positions of the partials were determined by calculating the density distribution of the Burgers vector, defined as

$$\rho(z) = \frac{d(\Delta u)}{dz} , \qquad (14)$$

where $\Delta u(z) = |u_A - u_B|$ is the displacement difference (also called disregistry or misfit) between the atoms in the adjacent $(\bar{1}11)$ planes above and below the slip plane. We have plotted $\Delta u(z)$ for copper in Fig. 1(b), and the corresponding $\rho(z)$ in Fig. 1(c). The width of the dislocation core w can be defined as the range of the z coordinate around the partial where the magnitude of the disregistry is less than $b/8$. The magnitude of the equilibrium separation between the partials can be easily estimated using the linear elasticity theory. By taking into account that the dissociated partials have both edge and screw components, the elastic estimate for the equilibrium separation is[44]

$$d_0^{el} = \frac{Br_0^2}{16\pi\gamma} \left[2 - \frac{3v}{1-v^2} \right] , \qquad (15)$$

where B is the bulk modulus, r_0 the nearest-neighbor distance, γ the stacking-fault energy, and v the Poisson's ratio, which is known to be about 0.3 for metals. Using the values evaluated from EMT for Al ($B = 86$ GPa, $r_0 = 5.43$ a.u., and $\gamma = 55$ ergs/cm^2), $d_0^{el} = 49$ a.u. ($9b$ in terms of Burgers vector). For Cu the corresponding values are $B = 185$ GPa, $r_0 = 4.67$ a.u., and $\gamma = 79$ ergs/cm^2 which gives $d_0^{el} = 53$ a.u. ($11.4b$). The equilibrium separation d_0 and the width of the dislocation core w for both Al and Cu are given in Table II together with some previous results calculated with empirical pair potentials or pseudopotentials. The equilibrium separations determined from the molecular-dynamics results are 46 ± 2 and 49 ± 2 a.u. for Al and Cu, respectively, in agreement with the elasticity theory. The error is estimated by comparing the values of d_0 obtained from two calculations for Al which use different cell sizes (see below), and is less than one
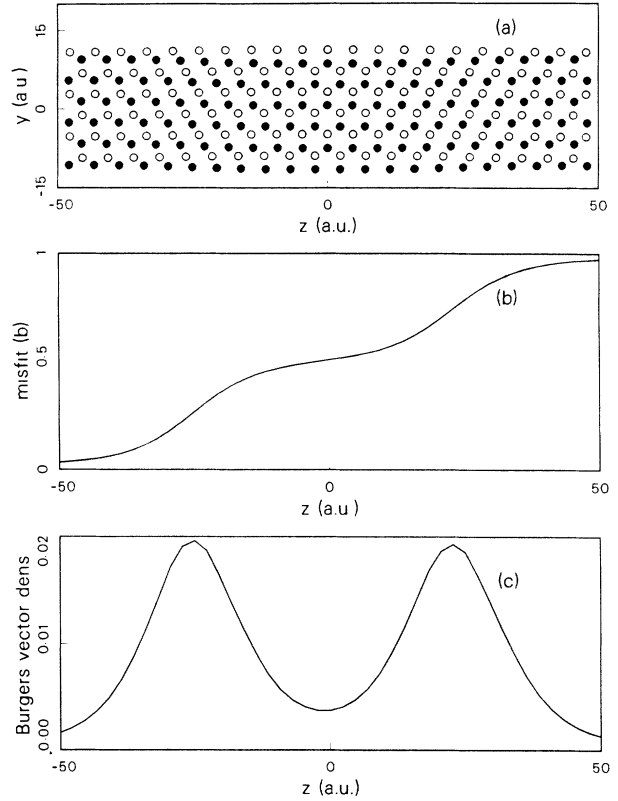

FIG. 1. The structure of the extended dislocation in Cu. (a) shows the atomic positions on the $(\bar{1}11)$ layers below (open circles) and above (solid circles) the slip plane. The atoms denoted with solid circles belong to the glide plane. (b) shows the misfit (disregistry) between the atomic planes shown in (a). The density distribution of the Burgers vector is plotted in (c). The position of the partials can be determined with the aid of (b) and (c), which are plotted in the same coordinate scale as (a). The difference in the stacking between and outside the partials as well as the lattice distortion in the $[1\bar{1}2]$ direction due to the stacking fault can be clearly seen in (a).

TABLE II. The comparison of the effective-medium results for Al and Cu with the previous pair-potential calculations for Cu. γ is the stacking-fault energy produced by the potential model, d_0 is the observed equilibrium separation between the partial dislocations, d_0^{el} is the elastic estimate for the partial separation, w is the core width (see text for the definition), and N is the number of dynamical atoms in the sample. b is the magnitude of the Burgers vector.

	Potential	γ (ergs/cm^2)	d_0 (b)	d_0^{el} (b)	w (b)	N
Al	EMT (this work)	55	8.5 (46±2 a.u.)	9 (49 a.u.)	3	7560
Cu	EMT (this work)	79	10.5 (49±2 a.u.)	11.4 (53 a.u.)	3	7560
	Morse[a]	31	8	7.2	5	≈4200
	Englert et al.[b]	70	9.2		5	504
	Englert et al.[c]	70	13		5	1120
	Dagens[d]	73	≈9			7776

[a]Reference 47.
[b]Reference 50.
[c]Reference 51.
[d]Reference 45.

(110) plane separation. Previous calculations for copper have also shown that the equilibrium distance between the partial dislocations is mainly determined by their elastic interaction[47,50,51] provided the sample has been large enough in the glide direction.[52] However, the EMT seems to produce a somewhat narrower dislocation core for partial dislocations in copper than the previous pair-potential calculations. The atomic displacements in the core region are sensitive to the potential, and our results may show effects from many-atom interactions which have been neglected in the previous calculations.

We find that the rigid surface layers perpendicular to the direction in which the partial dislocations are gliding do not give a noticeable effect on the observed equilibrium distance between the partial dislocations. We use the rigid surface layers according to our previous experience of test simulations of one partial dislocation. In these simulations the partial dislocation always escaped from the sample, if the surface perpendicular to its glide direction was free. This long-range attraction between the free surface and the partial dislocation is caused by an image force.[44] On the other hand, a dislocation is not likely to move in a vicinity of a rigid surface, because it cannot adjust itself to the large atomic displacements associated with the core region. To ensure that the rigid (110) surfaces do not stop the partial dislocations the sample was made extensive in the [110] direction. Moreover, we made an identical simulation for an Al sample with only half of the previous width of the cell in the [110] direction (the number of dynamical atoms was 3528). The density distribution of the Burgers vector obtained from this calculation is shown in Fig. 2, together with the corresponding density profile obtained from the simulation
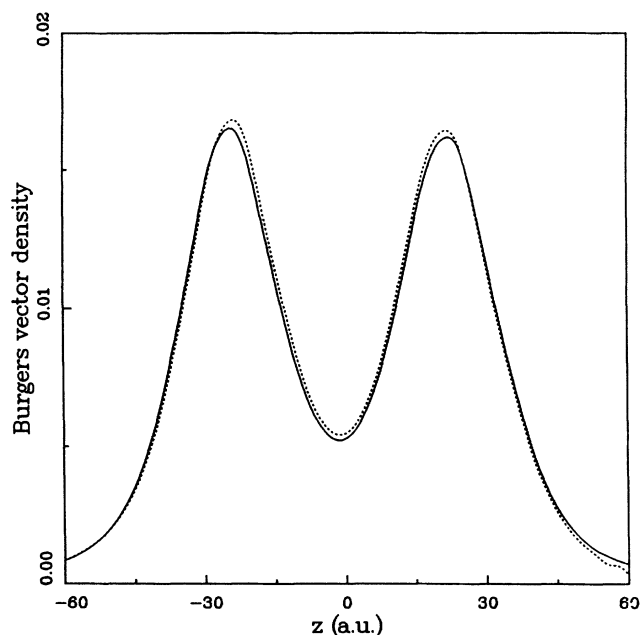

FIG. 2. The density distribution of the Burgers vector for Al calculated with the samples of 3528 (dotted line) and 7560 (solid line) dynamical atoms. The separation of the partials is the same within the accuracy of about 2 a.u., which is less than one (110) plane separation.

for the larger sample. As can been seen, the density profiles are almost identical, and the equilibrium distance between the partials is the same up to 2 a.u., which is less than one (110) plane separation. This ensures that the observed structure of the extended dislocation is determined by EMT, and not by the boundary conditions.

In addition to the rod geometry, we have also used the bulk geometry for aluminum. This leads to an edge dislocation dipole, which further dissociates into four Shockley partial dislocations as discussed in Sec. IV C. This calculation confirms our results for one isolated partial pair.

C. The edge dislocation dipole in Al

In order to test further the validity of our results for isolated partial pair we have also used completely different boundary conditions and sample preparation than that discussed above. This test was made for Al and it shows the ability of EMT and molecular dynamics to relax the sample, originally very far from equilibrium, to a physically reasonable state. We started with an ideal Al crystal (at the zero-temperature density) defined by the lattice vectors $8a[\bar{1}11]$, $(3a/2)[1\bar{1}2]$, and $14a[110]$ in the x, y, and z directions of the real space, respectively. Two adjacent (110) half planes were then removed from the sample after which the total number of atoms was 3960. This remaining crystal was then the starting configuration for a constant-pressure molecular-dynamics simulation. The periodic-boundary conditions were imposed in all directions, so the initial bulk crystal bulk crystal had a semi-infinite rectangular vacancy tube in the $[1\bar{1}2]$ direction. The velocities of the atoms were scaled such as to correspond to the temperature of 100 K, and the system was allowed to evolve dynamically under Parrinello-Rahman-type equations of motion.[53] The vacancy tube was observed to immediately collapse into a pair of perfect $(a/2)[110]$ edge dislocations separated by 12 atomic planes in the $[\bar{1}11]$ direction. Both of these edge dislocations further dissociated to Shockley partial dislocations, which then started to glide. All this happened during the first 2000 time steps (6 ps) of the simulation, during which the temperature was scaled to 100 K after every 15 time steps (0.045 ps). The sample was then cooled down during the next 6000 time steps (18 ps), and the system was allowed to evolve freely during the final 8000 time steps (24 ps). The total length of this three-stage simulation was thus 16 000 time steps corresponding to 48 ps in real time. The relaxation procedure is illustrated in Fig. 3, which shows the behavior of the potential energy, temperature, and volume during the simulation. At 100 K the determination of the partial separations is difficult, because the whole unit of the four partials is moving in the glide direction. The movement stopped during the cooling stage, and a well-defined equilibrium structure, thereby, resulted. The partial separations were determined from the density distribution of the Burgers vector as before. The relaxed positions of the four partials are shown in Fig. 4, where the simulation cell has been shifted in the $[\bar{1}11]$ direction for clarity. The separations between the partials are slightly different from each other being about 38 and 41 a.u. The shorter
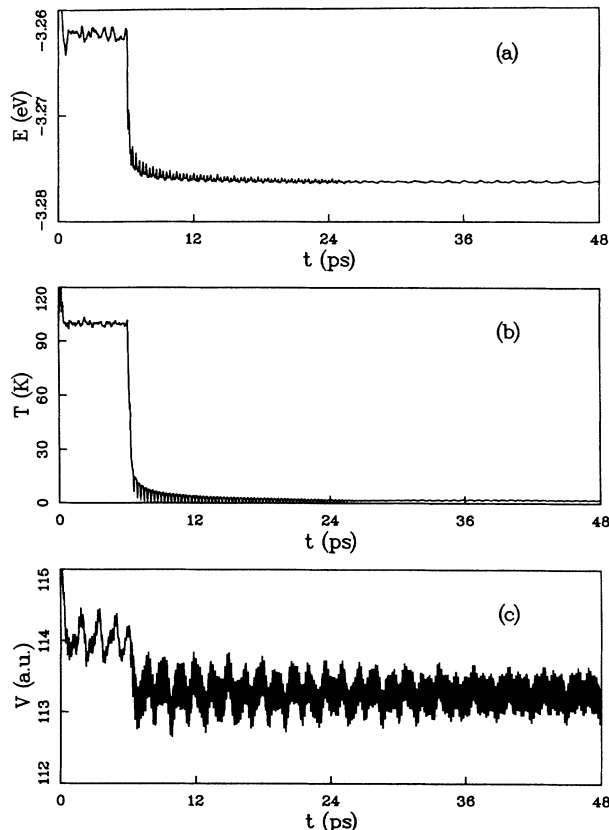
FIG. 3. The evolution of (a) the potential energy per atom E, (b) the temperature T, and (c) the atomic volume V during the three-stage simulation of the edge dislocation dipole in Al.
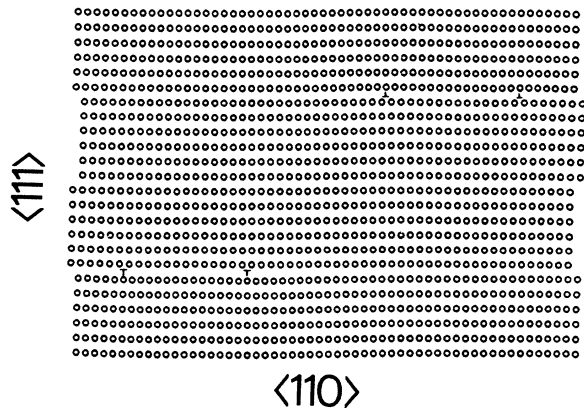

FIG. 4. The equilibrium structure of the extended edge dislocation dipole in Al. The slight distortion from 45° of the relative angle between the dipoles is due to the mutual interactions of the four partials. The computational cell is shifted in the $[\bar{1}11]$ direction to aid the visualization.

equilibrium distance than that found in Sec. IV B for one isolated partial pair in Al (46 a.u.) is clearly a result of the mutual interactions of the four partial dislocations. Figure 4 also shows that a general result of the linear elasticity theory holds: two edge dislocations with opposite Burgers vectors and different glide planes tend to form a relative angle of 45°. The equilibrium structure we find for the extended dislocation pair for aluminum agrees very well with the results of Tichy and Essman.[54] They used an iterative relaxation method and a semiempirical many-atom potential[15] to investigate the dislocation dipoles (of interstitial and vacancy type) in copper. They determined the total energy of various dislocation dipoles, and usually found many metastable configurations. The structure, which they found to give the lowest energy for the dislocation dipole separated by 12 (111) planes, is very close to the one obtained in this work.

D. Vacancy in the dislocation core

Dislocations in real metals always have point defects on the dislocation line. Point defects can diffuse into the core region from the undistorted parts of the crystal or they can be formed by collisions of moving dislocations. The behavior of the points defects in the dislocation core is drastically different from that in the bulk. The most

striking property is their fast diffusivity, which can have nearly liquidlike values close to the melting point. The (vacancy-type) point defects play an essential role also in the positron studies of dislocations, where the origin of the "medium-time" components (longer than the lifetime in the bulk but clearly shorter than the lifetime in a monovacancy) in the positron-lifetime spectra and the trapping mechanism have been subjects of controver-
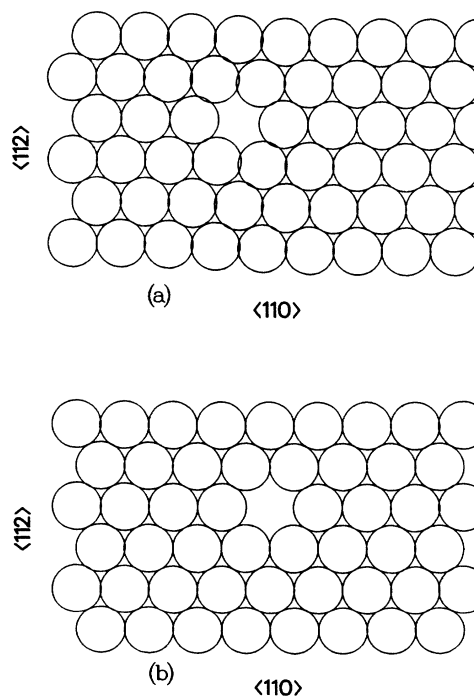

FIG. 5. Vacancy (a) on the partial dislocation line and (b) at the center of the stacking-fault region (in the glide plane) in Cu. The large asymmetric relaxation seen in (a) is caused by the unisotropic stresses originating in the stacking-fault region and in the ideal part of the lattice.

sy.[25−29] We shall return to this question in more detail in Sec. V. In this section we shall discuss the structural properties of a vacancy in the dislocation core in Cu with respect to a recently proposed model for the defect diffusion in the dislocation core.[45]

The relaxation of the vacancy is studied in this work with constant-volume molecular dynamics which start with the equilibrium configuration for an extended dislocation in a sample of 7992 atoms (Sec. IV B). In order to study the dependence of the relaxation on the position of the vacancy in the dislocation core we have considered two cases: a vacancy on the dislocation line of one of the partials, and a vacancy in the middle of the stacking-fault region in the glide plane. In both cases we have made a run of 4000 time steps (12 ps) and determined the average structure of the lattice during the last 2000 time steps (6 ps). The results are illustrated in Fig. 5, which shows the relaxation around the vacancy in the ($\bar{1}$11) glide plane. As can be seen in Fig. 5(a), the vacancy is significantly and asymmetrically relaxed on the dislocation line. This asymmetric relaxation is caused by the difference in the lattice stresses originating in the undistorted part of the crystal and in the stacking-fault region. On the other hand, the relaxation of the vacancy is symmetric in the middle of the stacking-fault region. This difference in the relaxation is seen also in the positron-lifetime calculations (Sec. V).

We have also estimated the vacancy formation energy by comparing the total energies of samples with and without the vacancy:

$$E_V^F = E(7991 \text{ atoms}) - \tfrac{7991}{7992} E(7992 \text{ atoms}) . \qquad (16)$$

The results for a vacancy on the dislocation line, in the middle of the stacking-fault region, and in the bulk are given in Table III. As expected, the vacancy formation energy on the dislocation line is smaller than that in the bulk. However, in the middle of the partial dislocations, E_V^F is larger than in the bulk. This is in qualitative disagreement with the results of Huang et al.[45] (also included in Table III). They used for copper a pseudopotential of Dagens[56] and calculated the vacancy formation energy at different positions in the core region. They concluded that the effective energy of vacancy formation is 0.3 eV lower in the core region and in the stacking-

TABLE III. The vacancy formation energy in the extended dislocation calculated from EMT for copper compared with the results obtained with the Dagens pseudopotential by Huang et al. (Ref. 45) and the experimental value in the bulk (Ref. 55). The value for the vacancy in the dislocation core reported in Ref. 45 is an effective formation energy calculated at several lattice positions in the core region.

	This work	Huang et al.	Expt.
Bulk	1.47	1.42	1.31
Partial dislocation line	1.33		
Center of the stacking fault	1.57		
Core region		1.15	

fault area than in the bulk. This means that there is considerable vacancy diffusion at the center of the stacking-fault area. They could also see this phenomena by the molecular-dynamics simulations. Our results would indicate that there is a large diffusion barrier between the partial dislocations, and fast diffusion could take place only in the narrow dislocation cores of the partial dislocations. In the EMT the vacancy formation energy is related to the embedding density. Figure 6 shows the embedding density as a function of the z coordinate in the ($\bar{1}$11) planes just above and below the slip plane. The maxima of the embedding density are located on the partial dislocation lines resulting in a clear minimum at the center of the stacking fault in the glide plane. Our results show that the vacancy diffusion is highly sensitive to the detailed core structure produced by the model potential. Huang et al.[45] observed a significant overlap of the partial dislocation cores [Fig. 1(c) in Ref. 45], which leads to a very narrow area where the stacking fault is ideal. In contrast with this, in our results the misfit is not so widely spread and, therefore, there is a well-defined area between the partial dislocations with an ideal stacking fault.

V. DISLOCATIONS AS POSITRON TRAPS

We determine first the energy and lifetime of the positron for perfect Al and Cu crystals. The lattice constants which we use in the calculations are given by the EMT results for Al and Cu at zero temperature (7.68 a.u. for Al and 6.60 a.u. for Cu). We use these lattice constants instead of the experimental lattice constants in order to make the results for the bulk and for the defected crystals
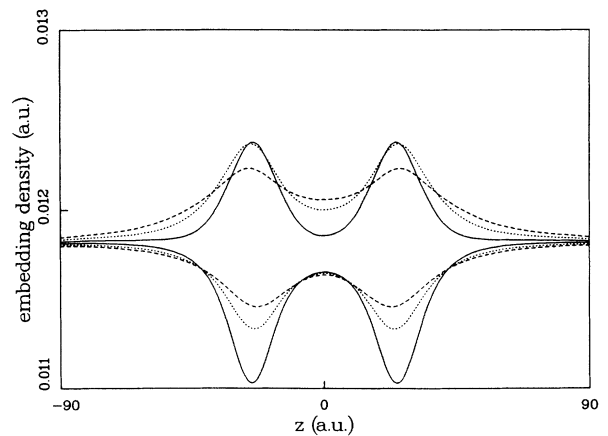

FIG. 6. The embedding density as a function of the z coordinate on the ($\bar{1}$11) planes above (upper curves) and below (lower curves) the slip plane in the regions of compressive and tensile stresses, respectively. The solid lines are for the planes adjacent to the slip plane, the dotted lines represent the second planes from the slip plane, and the dashed lines represent the third planes from the slip plane. The partial dislocation lines appear as the maxima of the embedding density in the glide plane (upper solid curve). The vacancies shown in Fig. 5 are in the glide plane. Note that in the stacking-fault region, the atoms in the second and in the third planes above the slip plane have a greater embedding density than those in the glide plane.

comparable. In the case of Al the calculated positron lifetime in the perfect crystal is 173 ps, a little bit longer than the experimental value of 163–166 ps.[57,58] When the slightly smaller experimental lattice constant (7.62 a.u.) is used, the calculated positron lifetime decreases to 170 ps. For Cu the measured lattice constant is 6.82 a.u., about 3% *longer* than the EMT value. However, in the latter case the calculated positron lifetime of 113 ps is almost the same as the experimental value of 110–112 ps.[59,60] By using the experimental lattice constant the calculated bulk lifetime for Cu is 125 ps.

In these calculations of the positron annihilation in perfect lattices, the unit cell was chosen to be a quadrangle consisting of three atomic layers in the [$\bar{1}11$] direction, six layers in the [$1\bar{1}2$] direction, and two layers in the [110] direction. A mesh was formed in the unit cell by dividing the distance between any two adjacent atomic layers into 16 segments in the [$\bar{1}11$] direction and into 8 segments in the other two directions ($N_x = 16$ and $N_y = N_z = 8$). In this way the separation between the nodes of the mesh [the h_l values in Eq. (9)] was, e.g. for Al, 0.14 Å in the [$\bar{1}11$] direction, 0.10 Å in the [$1\bar{1}2$] direction, and 0.18 Å in the [110] direction. In determining the Coulomb potential and the electron density inside the cell, the contribution of the atoms outside the cell was also taken into account. In the calculation of the positron wave-function, periodic-boundary conditions were imposed in all three directions.

In studying the trapping of the positron on the dislocation line, the boundary conditions for the positron wave function were changed to be periodic only in the direction of the line ([$1\bar{1}2$]). In the other directions the wave function was set equal to zero at the walls of the computational cell. The dimensions of the cell were, e.g., for Al, 10.6 Å in the [$\bar{1}11$] direction, 4.97 Å in the [$1\bar{1}2$] direction, and 8.62 Å in the [110] direction. Due to the large integration volume compared with those of the perfect lattices, the mesh was now slightly sparser: $N_x = 10$, and
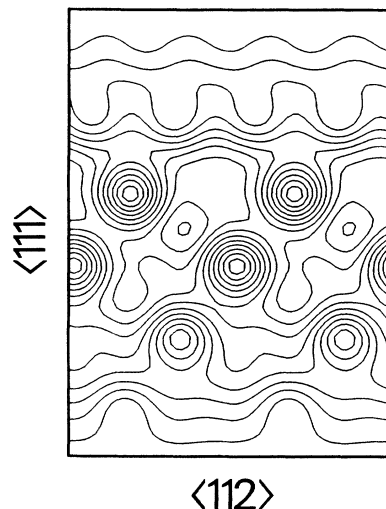

FIG. 7. The positron wave function on the partial dislocation line in Al. No significant trapping center can be seen in the core region.

$N_y = N_z = 5$. As can be seen in Fig. 7, the positron wave function on the dislocation line in Al is delocalized in the whole cell. No particular trapping center can be found in the core region of the dislocation, and the positron is free to move along the dislocation line. Note that localization which is perpendicular to the dislocation line, seen in Fig. 7, is mainly due to the boundary conditions: the wave function is zero at the ($\bar{1}11$)-cell boundaries.

In order to estimate the binding energy of the positron on the dislocation line, the calculation was carried out also for perfect crystals with the same boundary conditions. The binding energy was now obtained by subtracting the energy of the positron on the dislocation line from that in the perfect crystal with the same boundary conditions. The results are shown in Table IV, and they clear-

TABLE IV. The calculated positron lifetimes τ_{cal} compared to the experimental values τ_{expt}. V_{Al} and V_{Cu} correspond to the aluminum and copper vacancy, respectively. E_b is the calculated positron binding energy in the defect. Results for the Al(111) dislocation loop are from Ref. 61.

		τ_{cal} (ps)	τ_{expt} (ps)	E_b (eV)
Al	bulk	173	163,[a]166[b]	
	V_{Al}	252	245,[b]251[a]	2.0
	[$1\bar{1}2$] dislocation line	174		0.10
	[$1\bar{1}2$] dislocation line + V_{Al}	225	215,[c]230[d]	1.0
	[$1\bar{1}2$] dislocation line + jog	224		1.3
	(111) dislocation loop	191		0.4
Cu	bulk	113	110,[e]112[f]	
	V_{Cu}	185	165,[g]179[e]	1.6
	[$1\bar{1}2$] dislocation line	114		0.06
	[$1\bar{1}2$] dislocation line + V_{Cu}	166	155[h]	0.8
	V_{Cu} in the stacking-fault region	177		1.2

[a]Reference 58.
[b]Reference 57.
[c]Reference 24.
[d]Reference 21.
[e]Reference 59.
[f]Reference 60.
[g]Reference 62.
[h]Reference 63.

ly indicate that the pure dislocation line in both Al and Cu is only a shallow trap for positrons. The positron lifetimes are almost the same as in the bulk crystals: 174 ps in Al, and 114 ps in Cu, with the positron binding energies of 100 and 60 meV, respectively. A finite integration volume in this kind of calculation gives rise to an excessive kinetic energy of the positron. This effect is expected to be larger in the bulk than in a sample containing a dislocation. The calculated positron binding energies are then upper limits to the exact values.

Positron-annihilation characteristics were calculated also for dislocations containing a vacancy. In these calculations the positron wave function was set equal to zero at the walls of the calculation cell in all directions. In the [$\bar{1}11$] and [110] directions, the dimensions of the cell were the same as in the case of the pure dislocation line, but the cell contained two unit cells in the [$1\bar{1}2$] direction. The resulting positron wave function was strongly localized in the vacancy, although the open volume seen by
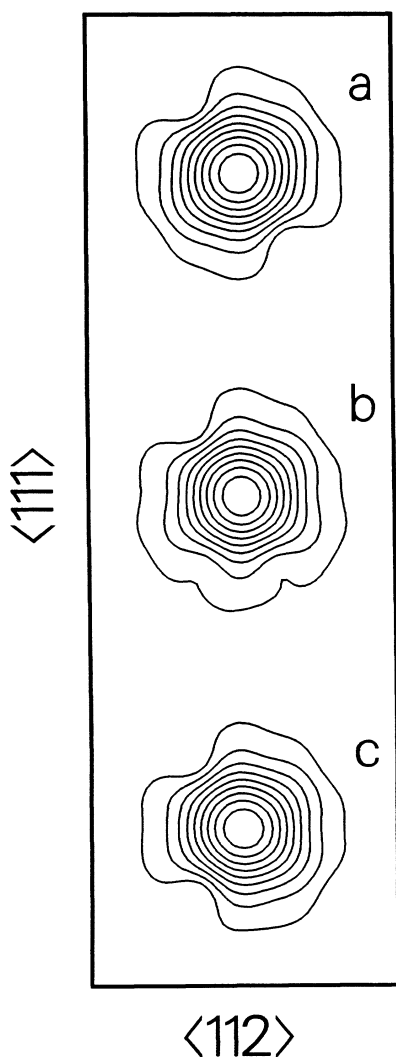

$\langle 112 \rangle$

FIG. 8. The positron wave function localized (a) in a Cu bulk vacancy, (b) in a Cu vacancy one the [$1\bar{1}2$] dislocation line, and (c) in a Cu vacancy in the stacking-fault region (in the glide plane) between the two partial dislocations.

the positron was smaller than in the case of the bulk vacancy (Fig. 8). The binding energy of the positron in this dislocation vacancy was 1.0 eV for Al, and 0.8 eV for Cu, clearly smaller than the values for the bulk vacancies which are 2.0 eV for Al and 1.6 eV for Cu. The positron lifetimes differed also significantly from those in the bulk vacancies. In Al a vacancy on the dislocation line resulted in a positron lifetime of 225 ps, while the lifetime in a bulk vacancy is 252 ps. For Cu the positron lifetime was 166 ps in a dislocation vacancy and 185 ps in a bulk vacancy.

In an earlier work[64] calculations were also performed for a row of six vacancies to mimic a jog on the dislocation line in Al. More vacancies would have been needed to get a separated jog structure. However, a tendency for localization of the positron in the jog region was observed. The positron lifetime was almost the same as that in a vacancy on the dislocation line which means that these two defects must be quite similar with respect to the volume available for the positron. The results clearly indicate that the long defect-related lifetimes seen in experiments with metal samples which contain dislocations, are those of positrons in vacancies or jogs on the dislocation line.

At low temperatures the dislocation line can be a precursor state for positrons which are going to trap at the point defects. The trapping rate can be estimated from the model calculations of Smedskjaer et al.[27] By estimating the width of the positron wave function to be 20 a.u. or more, and the binding energy to be about 0.1 eV, the result of Smedskjaer et al. gives a specific trapping rate of about 0.1 cm^{2}s^{-1} for both Al and Cu. This is in good agreement with the experimental estimate[21,65] 0.07–0.15 cm^{2}s^{-1} for Al, and strongly suggests that the dislocation line is a precursor state for the deeper traps which are observed experimentally.

The lifetime and the binding energy of the positron were also calculated for a Cu vacancy in the stacking-fault region between the two partial dislocation lines (see Sec. IV D). Although the atomic structure of the relaxed vacancy was almost identical to that of the bulk vacancy when looked from the [$\bar{1}11$] direction there were small differences in the structure when viewed from other directions. The positron lifetime was 177 ps, 8 ps shorter than the lifetime in a bulk vacancy, but still 11 ps longer than that in a vacancy on the dislocation line. The positron binding energy in a vacancy in the stacking-fault region, 1.2 eV, is also between those of a bulk vacancy (1.6 eV) and of a vacancy on the dislocation line (0.8 eV). The structural differences between the bulk vacancy and the vacancy on the dislocation line or in the stacking-fault region are clearly seen, if one compares the contour plots of the positron wave function localized in these defects (Fig. 8). The calculation of the positron wave function can also be viewed as an elegant way of studying the open volume structures of different kinds of defects.

In another simulation,[61] a vacancy-type dislocation loop in the (111) plane of Al was studied. The postiron was weakly localized in a corner of the loop with a binding energy of 0.43 eV and a lifetime of 191 ps. By combining all these various results, one can conclude that

dislocations in fcc metals provide a wide variety of different trapping sites for positrons, ranging from very shallow traps to strong vacancy-type traps. Therefore, a large number of different lifetimes is expected to be observed in deformed metals, varying from the lifetime in the bulk to that in a bulk vacancy.

VI. CONCLUSIONS

We have studied the structures of extended edge dislocations in fcc metals by using molecular-dynamics simulations and a many-atom long-range potential derived from the effective-medium theory. Our calculational method is able to describe the spontaneous dissociation of the perfect edge dislocation to Shockley partial dislocations. The resulting configuration is a dynamical equilibrium, where the separation and the core widths of the partial dislocations can be determined. The possible effects of the boundary conditions in the rod geometry have been eliminated by using large sample sizes in the glide direction. A simulation using bulk geometry confirms our results for the rod geometry. The observed separations of the partial dislocations in Al and Cu are consistent with the elasticity theory and with the theoretical stacking-fault energies. The results for copper are also consistent with those of the earlier pair-potential calculations. However, the core widths we find for Al and Cu are about $3b$, whereas all the pair potential calculations typically give widths which are close to $5b$. This difference may be a result of the many-atom effects in the core region.

We have also studied the collapse of the rectangular vacancy tube, and the resulting edge dislocation dipole in Al. The equilibrium structure is found to obey a general rule of the elasticity theory: two line dislocations with opposite Burgers vectors and different glide planes tend to move such that their relative angle becomes 45°.

In addition to the structure of the pure dislocation line,

we have also studied the relaxation of a vacancy on the dislocation line both in Al and Cu, and at the center of the stacking-fault region in Cu. The relaxation is found to be large and asymmetric on the partial dislocation line. This is caused by unisotropic stresses originating in the stacking-fault region and in the ideal part of the crystal. In Cu, the large relaxation on the dislocation line results in a lower vacancy formation energy than that in the bulk. On the other hand, the vacancy formation energy is higher in the middle of the stacking fault than in the bulk. This implies that fast vacancy diffusion can take place only in the narrow core region of the partial dislocations. This is in contrast with a recent proposal for fast diffusion also in the stacking-fault region, and indicates the sensitivity of the defect behavior to the details of the model potential.

Well-tested theoretical methods have been used to calculate the positron-annihilation characteristics in the pure dislocation core, and in the vacancy-type defects associated with it. The results show that the pure edge dislocation line is only a shallow trap, but it can be a precursor state to deeper traps. These deeper traps are pointlike vacancy-type defects. The positron lifetime components resulting from these defects are distinguishable from the lifetime coming from monovacancies in the bulk, and are in agreement with the experimentally observed lifetimes in deformed metals.

[1]See, e.g., J. Friedel, *Dislocations* (Pergamon, Oxford, 1964); F. R. N. Nabarro, *Theory of Crystal Dislocations* (Oxford University Press, Oxford, 1967).

[2]*Diffusion in Crystalline Solids,* edited by G. E. Murch and A. S. Nowick (Academic, Orlando, 1984).

[3]See, e.g., R. M. J. Cotterill, in *Ordering in Strongly Fluctuating Condensed Matter Systems,* edited by T. Riste (Plenum, New York, 1980); J. M. Kosterlitz, in *Phase Transitions in Surface Films,* edited by J. G. Dash and J. Ruvalds (Plenum, New York, 1980).

[4]*Dislocations in Solids,* Vol. 1 of *The Elastic Theory,* edited by F. R. N. Nabarro (North-Holland, Amsterdam, 1979).

[5]*Interatomic Potentials and Simulation of Lattice Defects,* edited by P. C. Gehlen, J. R. Beeler, Jr., and R. I. Jaffee (Plenum, New York, 1972).

[6]For a review of the pair-potential calculations of dislocations in metals, see V. Vitek, Philos. Mag. A **58**, 193 (1988).

[7]J. K. Nørskov and N. D. Lang, Phys. Rev. B **21**, 2131 (1980); M. J. Stott and E. Zaremba, *ibid.* B **22**, 1564 (1980).

[8]M. Manninen, Phys. Rev. B **34**, 8486 (1986).

[9]K. W. Jacobsen, J. K. Nøskov, and M. J. Puska, Phys. Rev. B **35**, 7423 (1987).

[10]M. S. Daw and M. I. Baskes, Phys. Rev. Lett. **50**, 1285 (1983), M. S. Daw, Phys. Rev. B **39**, 7441 (1989).

[11]M. W. Finnis and J. E. Sinclair, Philos. Mag. A **50**, 45 (1984).

[12]F. Ercolessi, E. Tosatti, and M. Parrinello, Phys. Rev. Lett. **57**, 719 (1986).

[13]J. von Boehm and R. M. Nieminen, Phys. Scr. (to be published).

[14]S. M. Foiles, M. I. Baskes, and M. S. Daw, Sandia National Laboratories Report No. SAND87-8903 (1988) (unpublished).

[15]G. J. Ackland, G. Tichy, V. Vitek, and M. W. Finnis, Philos. Mag. A **56**, 735 (1987).

[16]A. Bourret, J. Desseaux, and A. Renault, J. Microsc. Spectrosc. Electron **2**, 467 (1977).

[17]H. Hashimoto and Y. Takai, Bull. Jpn. Inst. Metals **22**, 595 (1983); Y. Takai, H. Hashimoto, and H. Endo, Acta Crystallogr. Sect. A **39**, 516 (1983).

[18]*Positrons in Solids,* Vol. 12 of *Topics in Current Physics,* edited by P. Hautojärvi (Springer, Heidelberg, 1979).

[19]*Postiron Solid State Physics,* Proceedings of the International School of Physics, "Enrico Fermi," Varenna, 1981, edited by W. Brandt and A. Dupasquier (North-Holland, Amsterdam, 1983).

[20]S. Berko and J. C. Erskine, Phys. Rev. Lett. **19**, 307 (1967)

[21]P. Hautojärvi, A. Tamminen, and P. Jauho, Phys. Rev. Lett. **24**, 459 (1970).

[22]Cs. Szeles, Zs. Kajcsos, and A. Vértes, Phys. Rev. B **31**, 1302 (1985).

[23]L. Diaz, R. Pareja, M. A. Pedrosa, J. I. Prieto, and R. González, Philos. Mag. A **51**, L61 (1985).

[24]C. Hidalgo, S. Linderoth, G. González-Doncel, and J. San Juan, in *Proceedings of the 8th International Conference on Positron Annihilation,* Ghent, 1988, edited by L. Dorikens-Vanpraet, M. Dorikens, and D. Segers (World Scientific, Singapore, 1989).

[25]J. W. Martin andR. Paetsch, J. Phys. F **2**, 997 (1972)

[26]M. Doyama and R. M. J. Cotterill, in *Proceedings of the Vth International Conference on Positron Annihilation,* edited by R. R. Hasiguti and K. Fujiwara (Japan Institute of Metals, Sendai, 1979).

[27]L. C. Smedskjaer, M. Manninen, and M. J. Fluss, J. Phys. F **10**, 2237 (1980).

[28]B. Bergensen and T. McMullen, Solid State Commun. **24**, 421 (1977).

[29]J. Arponen, P. Hautojärvi, R. Nieminen, and E. Pajanne, J. Phys. F **3**, 2092 (1973).

[30]M. J. Puska and R. M. Nieminen, J. Phys. F **13**, 333 (1983); for a review see M. J. Puska, Phys. Status Solidi A **102**, 11 (1987).

[31]M. J. Puska, S. Mäkinen, M. Manninen, and R. M. Nieminen, Phys. Rev. B **39**, 7666 (1989).

[32]K. W. Jacobsen and J. K. Nørskov, Phys. Rev. Lett. **59**, 2764 (1987); **60**, 2496 (1988); P. Stoltze, J. K. Nørskov, and U. Landman, Phys. Rev. Lett. **61**, 440 (1988).

[33]H. Häkkinen and M. Manninen, J. Phys. Condens. Matter **1**, 9765 (1989).

[34]M. J. Puska, R. M. Nieminen, and M. Manninen, Phys. Rev. B **24**, 3037 (1981).

[35]R. A. Johnson, in *Proceedings of the International Workshop on Many-Atom Interactions in Solids,* Pajulahti, 1989, edited by M. J. Puska, R. M. Nieminen, and M. Manninen (Springer-Verlag, Berlin, in press).

[36]*Theory of the Inhomogeneous Electron Gas,* edited by S. Lundqvist and N. H. March (Plenum, New York, 1983).

[37]B. Chakraborty and R. W. Siegel, Phys. Rev. B **27**, 4535 (1983)

[38]R. M. Nieminen, E. Boroński, and L. J. Lantto, Phys. Rev. B **32**, 1377 (1985); E. Boroński and R. M. Nieminen, *ibid.* **34**, 3820 (1986).

[39]D. M. Ceperley and B. J. Alder, Phys. Rev. Lett. **45**, 566 (1980); we use their local exchange-correlation functional as parametrized by J. Perdew and A. Zunger, Phys. Rev. B **23**, 5048 (1981).

[40]J. Arponen and E. Pajanne, Ann. Phys. (N.Y.) **121**, 343 (1979); J. Phys. F **9**, 2359 (1979).

[41]G. E. Kimball and G. H. Shortley, Phys. Rev. B **45**, 815 (1934)

[42]M. J. Puska and R. M. Nieminen, Phys. Rev. B **29**, 5382 (1984).

[43]W. Brandt and J. Reinheimer, Phys. Lett. **35A** 109 (1971).

[44]D. Hull and D. J. Bacon, *Introduction to Dislocations* (Pergamon, Oxford, 1984).

[45]J. Huang, M. Meyer, and V. Pontikis, Phys. Rev. Lett. **63**, 628 (1989).

[46]In fact, the bulk geometry leads to a set of parallel infinite stacking-fault planes, which do not interact.

[47]R. M. J. Cotterill and M. Doyama, Phys. Rev. **145**, 465 (1966).

[48]J. P. Simon, J. Phys. F **9**, 425 (1979).

[49]A. Nordsieck, Math. Comp. **16**, 22 (1962); C. Gear, *Numerical Initial Value Problems in Ordinary Differential Equations* (Prentice-Hall, Princeton, 1971).

[50]R. C. Perrin, A. Englert, and R. Bullough, in Ref. 5, p. 509.

[51]M. J. Norgett, R. C. Perrin, and J. E. Savino, J. Phys. F **2**, L73 (1972).

[52]The sample size affected the observed equilibrium distance in Ref. 50.

[53]M. Parrinello and A. Rahman, Phys. Rev. Lett. **45**, 1196 (1980).

[54]G. Tichy and U. Essmann, Philos. Mag. B **60**, 503 (1989).

[55]R. W. Siegel, in *Point Defects and Defect Interactions in Metals,* edited by J. I. Takamura, M. Doyama, and M. Kiritani (University of Tokyo Press, Tokyo, 1982).

[56]L. Dagens, J. Phys. F **7**, 1167 (1977).

[57]M. J. Fluss, L. C. Smedskjaer, M. K. Chason, D. G. Legnini, and R. W. Siegel, Phys. Rev. B **17**, 3444 (1978).

[58]H. E. Schaefer, R. Gugelmeier, M. Schmolz, and A. Seeger, in *Proceedings of the Vth Risø International Symposium of Metallurgy and Materials Science,* edited by N. H. Andersen, M. Eldrup, N. Hansen, D. J. Jensen, T. Leffers, H. Lillholt, O. B. Pedersen, and B. N. Singh (Risø National Laboratory, Risø, Denmark, 1984).

[59]H. E. Schaefer, W. Stuck, F. Banhart, and W. Bauer, in *Proceedings of the International Conference on Vancancies and Interstitials in Metals and Alloys,* edited by C. Ambromeit and H. Wollenberger (Trans Tech, Aedermannsdorf, Switzerland, 1986).

[60]K. O. Jensen, M. Eldrup, S. Linderoth, and J. H. Evans, in *Proceedings of the 8th International Conference on Positron Annihilation,* edited by L. Dorikens-Vanpraet, M. Dorikens, and D. Segers (World Scientific, Singapore, 1988).

[61]S. Mäkinen, H. Häkinen, and M. Manninen, Phys. Scr. (to be published).

[62]M. J. Fluss, L. C. Smedskjaer, R. W. Siegel, D. G. Legnini, and M. K. Chason, J. Phys. F **10**, 1763 (1980).

[63]T. K. Lepistö and V-T. Kuokkala, in *Proceedings of the Vth Risø International Symposium on Metallurgy and Materials Science,* edited by N. H. Andersen, M. Eldrup. N. Hansen, D. J. Jensen, T. Leffers, H. Lillholt, O. B. Pedersen, and B. N. Singh (Risø National Laboratory, Risø, Denmark, 1984).

[64]H. Häkkinen, S. Mäkinen, and M. Manninen, Europhys. Lett. **9**, 809 (1989).

[65]G. Aldi, A. Dupasquier, U. La Malfa, S. Re Fiorentin, and C. Regazzoni, J. Phys. F **12**, 2185 (1982).